Theoretical and Applied Fracture Mechanics 130 (2024) 104253

Contents lists available at ScienceDirect

Theoretical and Applied Fracture Mechanics

journal homepage: www.elsevier.com/locate/tafmec

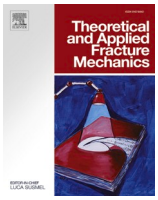

Performance of digital image correction technique for mild steel with different strain hardening effects

Bohua Zhang [a], Weigang Wang [a], Haoran Lei [a], Xiancun Hu [b], Chun-Qing Li [a,*]

[a] School of Engineering, RMIT University, Melbourne 3001, Australia
[b] School of Design and the Built Environment, University of Canberra, Canberra, ACT 2617, Australia

ARTICLE INFO

Keywords:
Digital image correlation technique
Unloading compliance method
Initial fracture toughness
δ-R curve
Strain hardening effects

ABSTRACT

This paper investigates the performance of Digital Image Correction (DIC) technique in determining the initial fracture toughness of mild steel with different strain hardening effects. To achieve this goal, the results of DIC technique-based method are compared with those of the commonly used unloading compliance (UC) method. The comparison results reveal that the DIC technique-based method exhibit a good agreement with the UC method in determining initial fracture toughness, with a deviation of less than 3.0 %. Additionally, the DIC technique-based method demonstrates the consistency in determining the initial fracture toughness, independent of the ratio of initial pre-crack length to width. Furthermore, the importance of strain hardening effects on initial fracture toughness follows the order of strain hardening capacity, effective yield stress, and yield offset. The significance of this paper is that it provides a deep understanding of the performance of the DIC technique in determining the initial fracture toughness of mild steel.

1. Introduction

Ductile materials, such as mild steel, are known for their capacity to undergo plastic deformation before fracturing, which makes them desirable for a wide range of structural and functional applications [2]. Understanding the fracture behaviour of ductile materials is crucial in ensuring the safety, reliability, and performance of engineering structures, as it directly impacts their mechanical behaviour and failure modes [30]. Moreover, the study of fracture behaviour of ductile materials enables the identification of root causes behind material failures, such as the formation of cracks and fractures in engineering components. It also provides valuable insights into strategies to prevent or mitigate similar failures in the future. Fracture toughness is a critical property of ductile materials, which is commonly used as a generic term for characterising the material resistance to crack growth [20].

The fracture behaviour of ductile materials is distinctly different from brittle materials due to the strain hardening effect, which results in increased resistance to crack extension in crack growth. Therefore, it is imperative to assess the fracture toughness of ductile materials using an entire crack extension resistance curve, such as the J-R or δ-R curve, rather than a single point value [24,38,42]. A J-R (or δ-R) curve can represent the changes of material resistance (i.e., characterized by J or δ) with crack extension Δa. The ASTM E1820-21 standard [3] provides guidelines for determining the J-R or δ-R curve through various experimental methods, including the conventional test method [22], unloading compliance method [8] and normalization method [17]. However, the conventional test method and the normalization method are not employed in this study because the former requires a significant number of specimens, and the latter is unsuitable for ductile materials with high strain hardening capacity such as mild steel [13]. Instead, the unloading compliance method, known for its high accuracy for measuring fracture toughness of ductile materials, especially in cases with significant plastic deformation and crack tip blunting [19], is utilized. The unloading compliance method, while considered reliable, demands a rigorous unloading–reloading procedure conducted on sophisticated equipment and is not conducive to harsh conditions, such as high loading rates, elevated temperatures, and corrosive environments [42].

The Digital Image Correction (DIC) technique is a non-contact method known for its high accuracy in determining real-time crack extension length and fracture parameters [35], which is often employed in the fracture toughness tests, e.g., [40,31,1], etc. However, there is a lack of comprehensive studies on the performance of the DIC technique for determining the initial fracture toughness of mild steel. Furthermore, it is well-known that the fracture toughness of ductile materials is

* Corresponding author.
E-mail address: chunqing.li@rmit.edu.au (C.-Q. Li).

https://doi.org/10.1016/j.tafmec.2024.104253
Received 28 October 2023; Received in revised form 1 January 2024; Accepted 3 January 2024
Available online 9 January 2024

Nomenclature

a_0	initial pre-crack length
a_f	final crack extension length
B_e	effective specimen thickness
B_N	net specimen thickness
C_i	elastic compliance at the beginning of the *ith* loading–unloading cycle
D	one-half of the initial distance between the LLD measurement points
E	Yong's modulus
H^*	initial half-span of the loading points, i.e., the centre of pin holes
$J_{el(i)}$	elastic part of J_i
J_i	*J*-integral at the beginning of the *ith* loading–unloading cycle
$J_{pl(i)}$	plastic part of J_i
m	a plastic constraint factor
n	strain hardening exponent
P_i	load at the beginning of the *ith* loading–unloading cycle
R_i	radius of rotation of the crack centreline, i.e.,$R_i = (W+\Delta a_i)/2$
V_i	LLD at the beginning of the *ith* loading–unloading cycle
$V_{pl(i)}$	plastic part of LLD at the beginning of *ith* loading–unloading cycle
W	specimen width
α	dimensionless constant
σ_{ys}	yield strength
σ_Y	effect yield stress
δ	crack tip opening displacement
δ_c	critical value of crack tip open displacement at fracture initiation
$\delta_{Ic-\mathrm{ASTM}}$	initial fracture toughness determined by the UC method
δ_{5c}	initial fracture toughness determined by the DIC-based method
θ	angle of rotation of a rigid body element about the unbroken midsection line
ε_y	strain component normal to the plane of the pre-existing crack
Δa_i	crack extension length at the beginning of the *ith* loading–unloading cycle
Δa_{ci}	corrected crack extension length at the beginning of the *ith* loading–unloading cycle
CT	compact-tension
CTOD	crack tip opening displacement
DIC	digital image correction
LLD	load line displacement
J-R	*J*-based fracture resistance
UC	unloading compliance
δ-*R*	δ-based fracture resistance

influenced by various factors [2], such as material composition and microstructure, loading rate and mode, environmental temperature, strain hardening effect, and specimen geometry. The strain hardening, also known as work hardening, is a fundamental phenomenon that occurs in ductile materials during plastic deformation. When a crack propagates through a ductile material, the strain hardening effect causes plastic deformation to occur around the crack tip, resulting in crack tip blunting [29,25]. Since more energy is absorbed by this plastic zone, it assists the material resistance to fracture initiation and further crack propagation, thereby enhancing the fracture toughness. The strain hardening behaviour of ductile materials can be characterized by several mechanical parameters, including effective yield stress, strain hardening capacity, and yield offset [15,2]. Previous research has investigated the influence of the strain hardening capacity on the fracture toughness of ductile materials, as demonstrated by studies conducted by Gao et al. [13], Liu et al. [24] and English and Arakere [11]. However, there is a lack of studies that comprehensively examines the effects of effective yield stress, yield offset, and strain hardening capacity on the fracture toughness of ductile materials.

In this paper, the DIC technique is employed to conduct fracture toughness tests and determine the initial fracture toughness of four grades of mild steel, i.e., G250, G350, PT460NR and A516-70. Then, the results obtained from the DIC technique-based method are compared with those of the unloading compliance (UC) method. Additionally, a comprehensive investigation is undertaken to study the influences of strain hardening parameters, including effective yield stress, strain hardening capacity and yield offset, on the fracture toughness measurements. This study primarily focuses on the influence of strain hardening using compact-tension (CT) specimens under mode-I loading conditions at room temperature with a quasi-static loading rate. Furthermore, this study evaluates the factors that affect the agreement of fracture toughness measurements obtained by these two methods.

2. Experimental program

In this section, two distinct fracture toughness test methods, i.e., the Digital Image Correction (DIC)-based fracture test method and the commonly used unloading compliance (UC) method, are elucidated. In the DIC technique-based fracture tests, the fracture initiation is detected by monitoring the changes in strain around the crack tip. In the UC method, the fracture initiation is determined by the intersection of a 0.2 mm offset line with the δ-*R* curve. These two test methods are conducted on four grades of mild steel (i.e., G250, G350, PT460NR and A516-70) to evaluate their corresponding initial fracture toughness.

2.1. Specimens

Tensile tests are conducted on the dog-bone specimens designed in accordance with the ASTM E8/E8M-16a standard [43]. Since this paper mainly focus on the study of the performance of DIC technique for mild steel with different strain hardening effects, the effects of specimen geometries, e.g., width and thickness, are not considered. Therefore, the standard compact-tension (CT) specimen (Fig. 1) with a 10 mm thickness, designed as per the ASTM E1820-21 standard [3], is utilized for the fracture toughness tests. Additionally, according to the ASTM E1820-21 standard [3], the tested specimens should be under the plane strain condition. 10 mm thickness is thick enough to achieve a plane strain condition [12–14]. Furthermore, to minimize excessive deformation on the pin holes during the loading process, loading fixtures are manufactured using high strength steel (HARDOX 450) and assembled with grade 12.9 steel bolts.

According to the ASTM E1820-21 standard [3], fatigue tests are conducted for all CT specimens to obtain a pre-crack length. The fatigue test is a commonly used and reasonable method for obtaining a pre-crack length, which has been employed in many studies (e.g., [42,44,45,46]). The ratio of initial pre-crack length (a_0) to the specimen width (W), i.e., a_0/W, are controlled in a range of 0.45–0.70. Subsequently, the specimens are sandblasted using 120 grit dry garnet at a pressure of 80 psi and a distance value of 400 mm. DIC painting is then applied to one side of the specimen surfaces, where flat black speckles are randomly sprayed on a thin layer of flat white coating.

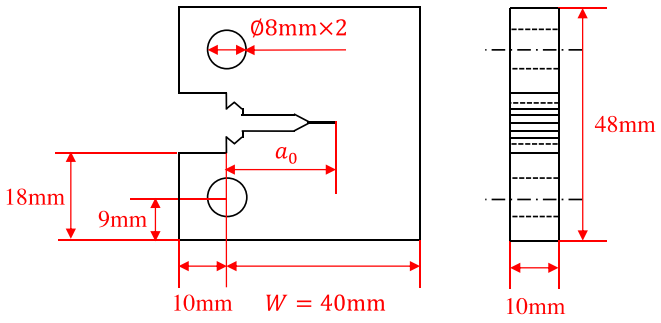

(a) CT specimen

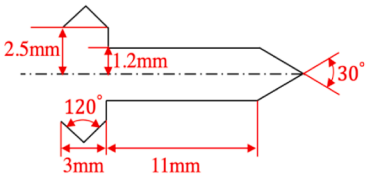

(b) notch

Fig. 1. The specimen prepared for the fracture toughness tests.

2.2. Tensile test

A Shimazu UH-F 500kN loading machine is utilized for conducting tensile tests with a constant displacement-controlled loading rate of 0.1 mm/min. To monitor the displacement changes, an extensometer (Epsilon Model 3542 with a gauge length of 50 mm) is affixed to the specimen. Four duplicate specimens are tested for each grade of mild steel, and the obtained engineering stress–strain curves are nearly the same. To be convenient for the following analysis, the mean values of these obtained engineering stress–strain data are used for constructing the final engineering stress–strain curves, as depicted in Fig. 2. Then, according to Fig. 2, the mechanical parameters are determined following the methodology outlined by Davis [9], as summarized in Table 1.

It is noted that the DIC technique may be more accurate than the extensometer for constructing the stress–strain curves in tensile tests. However, it is not employed in this study since the limitation of the used loading machine, in which the space for setting up the DIC system is not sufficient. This does not mean that the obtained stress–strain curves and mechanical parameters are not accurate enough because the test is conducted based on the ASTM E8/E8M-16a standard [43] and data is analysed based on the tensile test book [9].

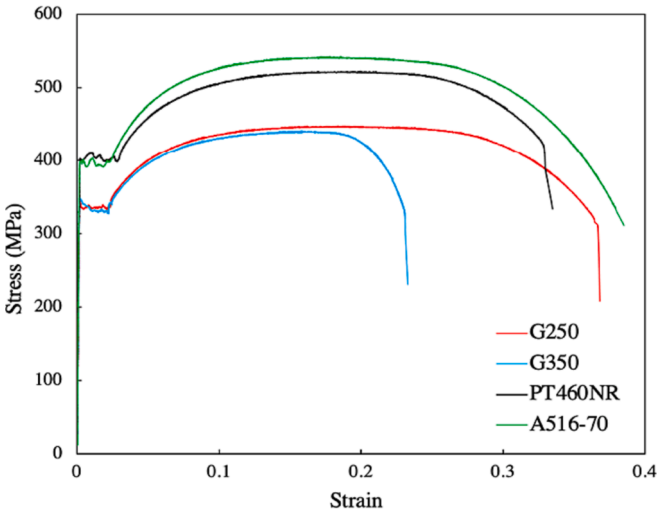

Fig. 2. Engineering stress–strain curves of tested mild steel.

To model the strain hardening behaviour of ductile materials, the Ramberg-Osgood power-law model is utilized, which involves two parameters, i.e., α and n, as elucidated by Anderson [2]. The true stress–strain data is fitted as follows:

$$\varepsilon_t = \frac{\sigma_t}{E} + \alpha \frac{\sigma_{ys}}{E} \left(\frac{\sigma_t}{\sigma_{ys}} \right)^n \tag{1}$$

where E represents the Yong's modulus, α is the dimensionless constant, n is the strain hardening exponent, σ_{ys} represents the yield stress, ε_t and σ_t represent the true strain and stress, respectively.

$\alpha \frac{\sigma_{ys}}{E}$ represent the yield offset. The strain hardening exponent (n) and the strain hardening capacity $(1/n)$ are reciprocal, in which a small value of $1/n$ signifies a lower strain hardening capacity. The values of α and n for each grade of mild steel are calculated based on Equation (1) and presented in Table 1. Notably, the calculated values of α are significantly larger than 1.0, indicating that the strain corresponding to the yield strength σ_{ys} is considerably larger than 0.2 %, in accordance with findings by Chattopadhyay [6] and Davis [9]. This paper presents a comprehensive investigation into the performance of DIC technique-based fracture toughness test method for mild steel, considering the strain hardening effects, which specifically focus on strain hardening capacity $(1/n)$, yield offset $(\alpha \frac{\sigma_{ys}}{E})$ and effect yield stress (σ_Y).

2.3. DIC technique-based method

A servo-hydraulic MTS 100KN loading machine is utilized for conducting DIC-based fracture tests, with a constant displacement-controlled loading rate set at 0.5 mm/min. A high-performance camera, specifically a Canon EOS 5D Mark III camera with a resolution of 22.3 megapixels and a 24–105 mm lens, is used to record the fracture process at a frequency of 1 Hz. The VIC-2D software is employed for analysing the fracture behaviour of mild steel, which facilitates the measurement of load line displacement (LLD), crack tip opening displacement (CTOD), and the detection of fracture initiation.

2.3.1. Measurement of load line displacement (LLD)

The load line displacement (LLD) is a crucial parameter for constructing δ-R curves. In experiments conducted under mode-I loading conditions, the crosshead displacement of the loading machine is commonly utilized as the LLD. Nevertheless, this approach may result in an overestimation of the plastic deformation that is necessary for fracture initiation, attributable to the stiffness of the machine, specimen deformation at loading points and specimen rotation [26]. In this study, the LLD is measured using the DIC technique by monitoring the displacement changes of a virtual extensometer along the direction of the applied load.

2.3.2. Measurement of crack tip opening displacement (CTOD)

For ductile materials, since plastic deformation around the crack tip dominates and material resistance increase as the crack grows, the fracture toughness is commonly characterised by the fracture parameters J-intergral or crack tip opening displacement (CTOD) [2]. For pre-fatigue prepared specimens (i.e., single-edge notched specimen in three-opine bending SE(B), compact-tension (CT) and arc-shaped bending A(B)) with the pre-crack ratios (i.e., initial pre-crack length (a_0) to the specimen width (W)) of $0.45 \leq a_0/W \leq 0.70$, there is a linear relationship between J-intergral and CTOD [3,10,34]. Therefore, these two fracture parameters are equally effective for characterising fracture behaviours of ductile materials, and CTOD can be used as an alternative to J-integral. The concept of CTOD (δ) was first proposed by Wells [47],

Table 1
A summary of mechanical properties for tested mild steel.

Steel grade	E (GPa)	σ_{ys} (MPa)	σ_{us} (MPa)	n	α	$\alpha\frac{\sigma_{ys}}{E}(\times 10^{-3})$	Elongation (%)
G250	208	336	447	6.65	6.08	9.822	36.3
G350	204	333	437	7.30	5.85	9.549	23.7
PT460NR	207	398	521	6.67	5.91	11.363	33.0
A516-70	209	401	543	5.45	6.05	11.608	38.5

in which fracture is assumed to occur when the measured δ exceeds a critical value δ_c, i.e., $\delta \geq \delta_c$. As CTOD varies with the crack extension, a CTOD-resistance (δ-R) curve can be constructed to describe the resistance of ductile materials to crack extension. In this study, the δ_5 method [39,33,16] is adopted to measure CTOD using the DIC technique. As illustrated in Fig. 3, two points with a span of 5 mm, located at opposite sides of the crack tip, are used to measure δ.

2.3.3. Determination of initial fracture toughness

In ductile materials, the strain in the vicinity of the crack tip typically increases with increasing load, and then sharply decreases upon the release of concentrated stress caused by crack extension [39,27]. The initial occurrence of a sudden reduction in strain serves as an indicator of the onset of crack growth, also known as fracture initiation. In the context of mode-I loading conditions, where the crack generation is induced by tension, the strain component normal to the plane of the pre-existing crack, denoted by ε_y, is utilized as a reliable parameter for detecting fracture initiation, as demonstrated by Van Minnebruggen et al. [37]. Specifically, as shown in Fig. 3, two points located 2 mm apart and crossing the pre-crack tip are utilized to measure the changes in ε_y. Simultaneously, the time corresponding to the peak value of ε_y is recorded to determine the load-line displacement (LLD) and the crack tip opening displacement (CTOD) at fracture initiation.

2.4. Unloading compliance method

The compact-tension (CT) specimens, as illustrated in Fig. 1, are also utilized in the fracture test based on the unloading compliance (UC) method. A servo-hydraulic MTS 100KN loading machine is also employed for conducting these fracture tests, following a loading–unloading test procedure. A crack opening displacement (COD) gage (Epsilon model-3451C with a gauge length of 5 mm) is attached to the crack mouth of CT specimens to continuously measure the load line displacement (LLD). Three duplicates are performed for each grade of steel to ensure test reliability.

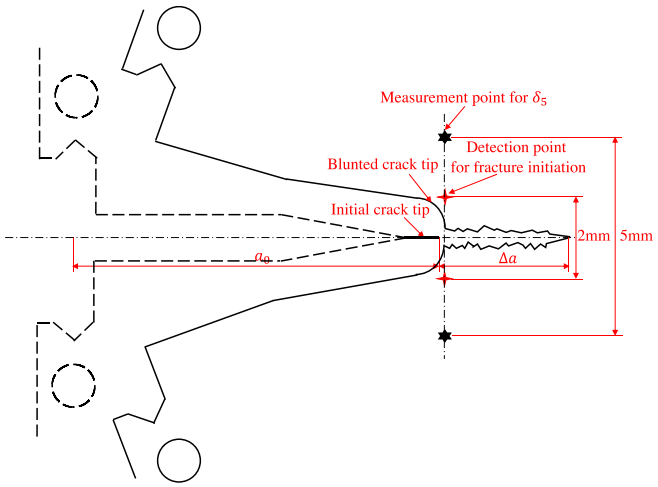

Fig. 3. Illustration of δ_5 measurement and fracture initiation detection.

2.4.1. Construction of δ-R curve

In the Unloading Compliance (UC) method, periodic small elastic unloading is applied to the specimen throughout the entire testing process. The compliance of unloading increases in proportion to the crack extension, as the stiffness of the specimen decreases.

The η_{pl} factor method is used for the determination of J-integral in the unloading compliance method [7]. The J-integral value (J_i) corresponding to the corrected crack extension length (Δa_{ci}) can be expressed as follows:

$$J_i = J_{el(i)} + J_{pl(i)} \tag{2}$$

where the subscript (i) denotes the ith loading–unloading cycle in the unloading compliance method, $J_{el(i)}$ and $J_{pl(i)}$ are elastic and plastic part of J_i, which can be determined as Appendix A. Additionally, as per ASTM E1820-21 standard [3], the crack extension length (Δa_i), i.e., at the beginning of the ith loading–unloading cycle, can be estimated by the changes in the corresponding corrected elastic compliance (C_i), which is summarized in Appendix B.

Then, the crack tip opening displacement δ_i, corresponding to J_i, can be determined as follows:

$$\delta_i = \frac{J_i}{m\sigma_Y} \tag{3}$$

with

$$m = A_0 - A_1\left(\sigma_{ys}/\sigma_{us}\right) + A_2\left(\sigma_{ys}/\sigma_{us}\right)^2 - A_3\left(\sigma_{ys}/\sigma_{us}\right)^3 \tag{4}$$

where σ_Y represents the effective yield stress, i.e., the average value of yield stress and ultimate stress, σ_{us} represents the ultimate stress, and m represents a plastic constraint factor which is associated with the strain hardening capacity of a material and typically falls within the range 1.0–2.0 [18], $A_0 = 3.62$, $A_1 = 4.21$, $A_2 = 4.33$ and $A_3 = 2.00$ for the CT specimens. Consequently, a δ-R can be constructed when δ_i corresponding to each crack extension length (Δa_{ci}) is determined.

2.4.2. Determination of initial fracture toughness

A construction line, i.e., $\delta_i = 2\Delta a_{ci}/m$, is drawn. Then, two exclusion lines parallel to the construction lines are drawn, intersecting the abscissa at 0.15 mm and 1.5 mm, respectively. The data points $(\delta_i, \Delta a_{ci})$ falling within the region enclosed by these two exclusion lines and capped by $\delta_{limit} = (W - a_0)/7.5m$ are considered as available data points. These selected data points are then fitted using a power-law relationship model, i.e., $\delta_i = K_1(\Delta a_{ci})^{K_2}/m\sigma_Y$ with coefficients K_1 and K_2, to construct an effective δ-R curve.

The initial fracture toughness is commonly determined by the intersection of a 0.2 mm offset line and the δ-R curve. The location of this 0.2 mm offset line is specified according to different standards, e.g., offsetting the construction line as per the ASTM E1820-21 standard [3], offsetting a blunting line (with a slope equalling the elastic part of δ-R curve) or a vertical line located at $\Delta a = 0$ both as per the [5] standard. Based on the above analysis, it can be concluded that the evaluation of initial fracture toughness depends not only on the selection of fracture test methods used for constructing the δ-R curves but also on the standards used for determining the 0.2 mm offset line.

3. Results and analysis

3.1. Results of the DIC technique-based method

Drawing from the methodology elucidated in Section 2.3.3 for detecting fracture initiation, the strain component (ε_y), i.e., corresponding to the first discernible decrease, is identified for each tested specimen. Specifically, by measuring the changes of the strain component (ε_y) on the detection points of fracture initiation (i.e., in Fig. 3), the ε_y vs. load line displacement (LLD) curve is constructed as Fig. 4. Then, according to Fig. 4, the strain component (ε_y) increases with the increasing of load line displacement, which reaches the peak value (i.e., marked as the red point) and then decreases. The location of the red point is identified as the fracture initiation.

Based on the methodologies elucidated in Section 2.3.1 and Section 2.3.2 for measuring LLD and CTOD respectively, the LLD-CTOD curves are constructed for each grade of mild steel as depicted in Fig. 5. The points denoted in red on the curves indicate the positions of fracture initiation, which are determined based on the findings from Fig. 4. According to Figs. 4 and 5, it can be found that the obtained ε_y-LLD curves and CTOD-LLD curves are not exactly same for the duplicate specimens of each grade of steel. This is mainly affected by the quality of DIC painting and the accurate locations of points for the measurement of ε_y and CTOD.

A summary of the initial fracture toughness values obtained by the DIC technique-based method is presented in Table 2. The findings revealed that the values of initial fracture toughness obtained by this method remain relatively consistent for each grade of mild steel, with a standard deviation (SD) ranging from 0.0016 to 0.0041. Furthermore, it was found that the values of initial fracture toughness obtained through the DIC technique-based method exhibit independence on the ratio of initial pre-crack length to width (a_0/W).

3.2. Results of the unloading compliance method

After fracture tests, as presented in Fig. 6, the nine-point averaging method is employed to directly measure the initial crack length a_0 and final crack extension length a_f from the fracture surfaces. The measured a_0 and a_f are summarized in Table 3. With the measured LLD obtained by COD gage, the load-LLD curves using the unloading compliance

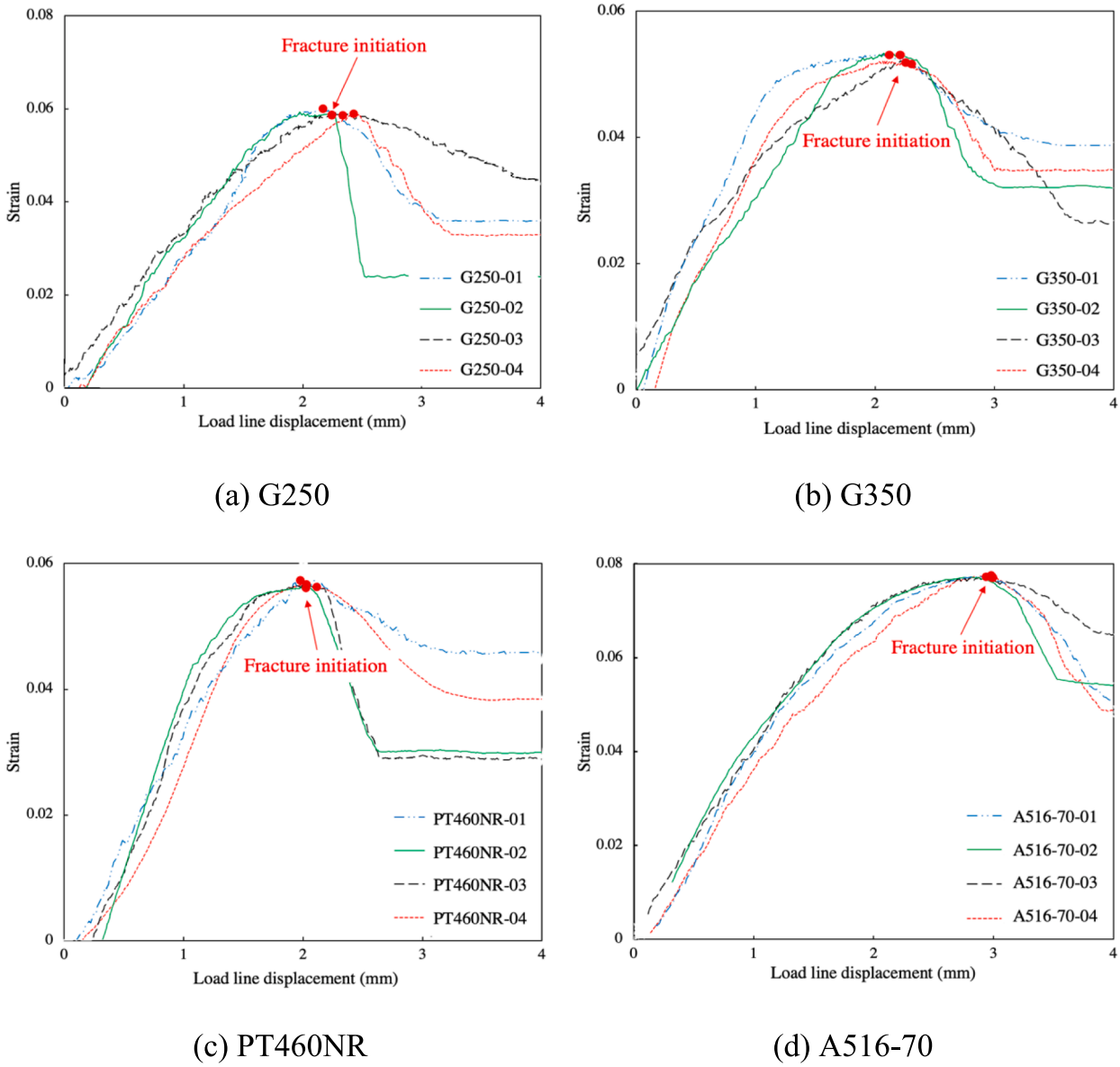

Fig. 4. Detection of fracture initiation for tested mild steel.

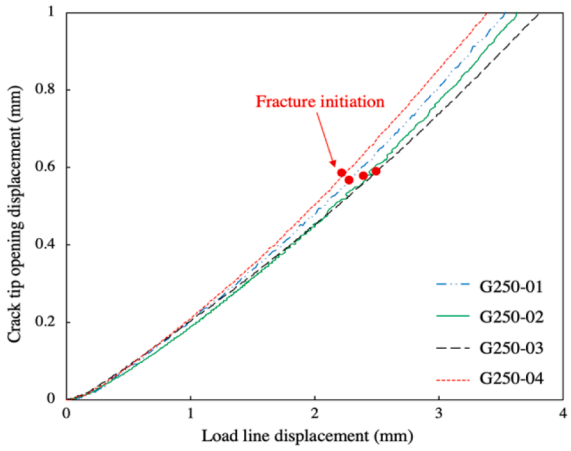

(a) G250

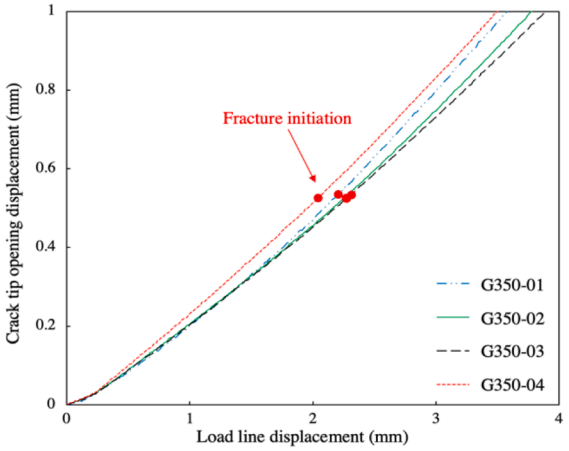

(b) G350

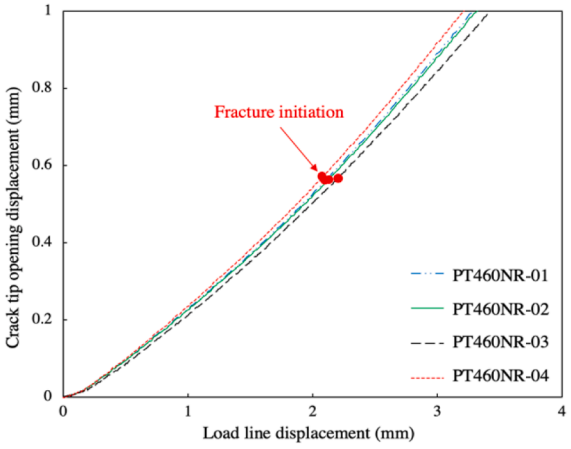

(c) PT460NR

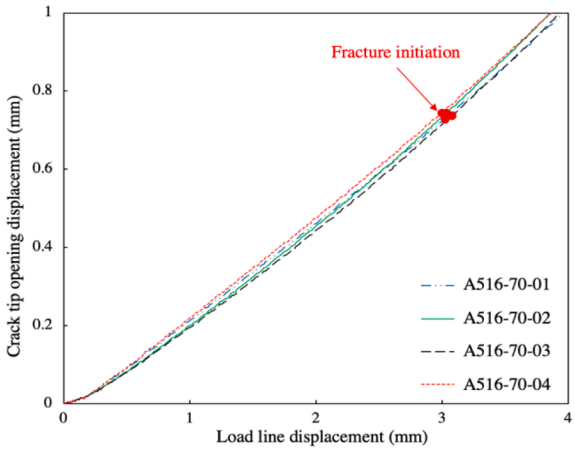

(d) A516-70

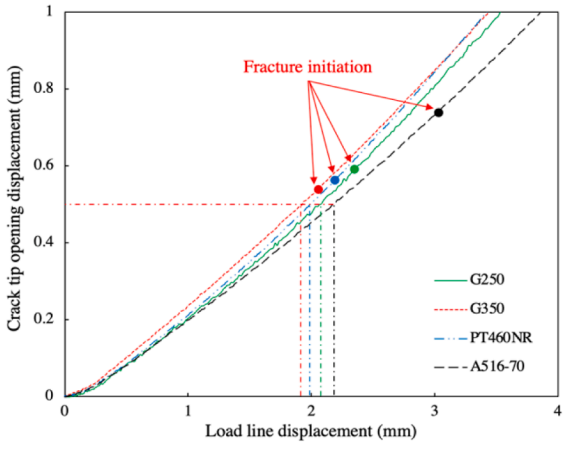

(a) Comparison

Fig. 5. LLD-CTOD curves constructed for tested mild steel.

Table 2
A summary of initial fracture toughness determined by the DIC technique-based method.

Steel grade	Specimen No.	$\frac{a_0}{W}$	δ_{5c} (mm)	Mean of δ_{5c} (mm)	SD of δ_{5c} (mm)
G250	01	0.517	0.5950	0.5913	0.0041
	02	0.525	0.5850		
	03	0.559	0.5900		
	04	0.508	0.5950		
G350	01	0.563	0.5250	0.5264	0.0021
	02	0.565	0.5300		
	03	0.581	0.5255		
	04	0.529	0.5250		
PT460NR	01	0.493	0.5700	0.5648	0.0034
	02	0.505	0.5615		
	03	0.517	0.5620		
	04	0.469	0.5655		
A516-70	01	0.534	0.7340	0.7330	0.0016
	02	0.540	0.7320		
	03	0.546	0.7350		
	04	0.514	0.7310		

method are constructed for each tested specimen and presented in Fig. 7. Then, the δ-R curves can be constructed, and initial fracture toughness can be determined based on the methodology outlined in Section 2.4.1 and 2.4.2, respectively. Consequently, Fig. 8 presents the δ-R curves constructed, and the initial fracture toughness determined for each tested specimen. Then, based on the ASTM E1820-21 standard [3], a summary of initial fracture toughness ($\delta_{Ic-ASTM}$) determined by the UC method is presented in Table 3. It is noted that, according to Fig. 7, although three duplicate specimens have been conducted for each grade of steel, the obtained load-LLD curves are not exactly same. Similarly, according to Fig. 8, the constructed δ-R curves of duplicate specimens are not exactly same. This is mainly because that it is difficult to control the ratios of initial pre-crack length to width (i.e., a_0/W in Table 3) as a same value. For example, as shown in Fig. 7, the measured load-LLD curve of the specimen G250-02 (i.e., $a_0/W = 0.542$) is higher than that of G250-03 (i.e., $a_0/W = 0.573$), because more plastic deformation is generated around the crack tip of the specimen G250-2, which absorbs a greater amount of energy (i.e., the area under load-LLD curve) before fracture initiation. Therefore, it was found that the values of $\delta_{Ic-ASTM}$ obtained through the UC method displayed inconsistency, being dependent on the corresponding values of a_0/W.

3.3. Effects of strain hardening on the evaluation of initial fracture toughness

As presented in Fig. 9, a comparative analysis of initial fracture toughness determined by the DIC technique-based method and the UC method is made for various grades of mild steel. The results revealed that the initial fracture toughness (δ_{5c}) obtained through the DIC technique-based method exhibited more consistency than those ($\delta_{Ic-ASTM}$) obtained through the UC method, with a reduced dependence on the ratio of initial pre-crack lengths to width (a_0/W).

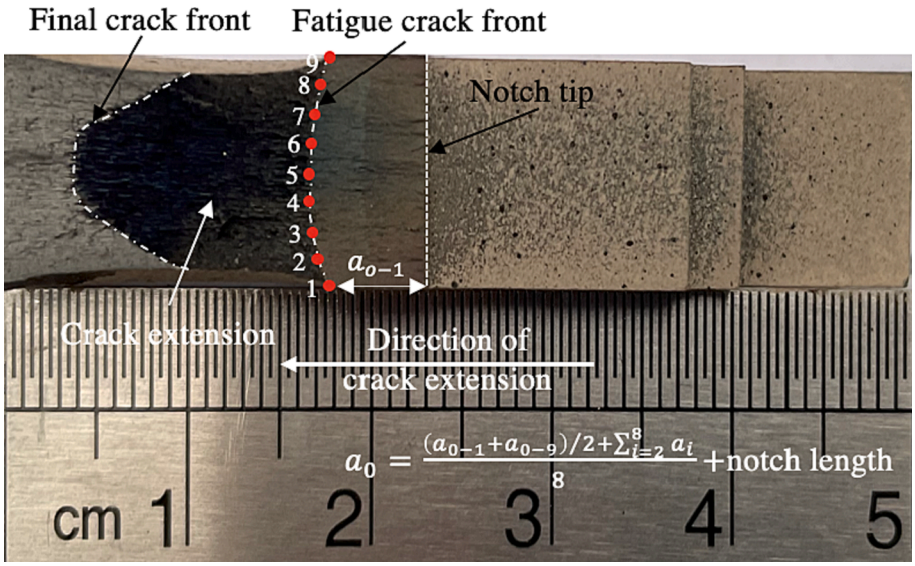

Fig. 6. Schematic illustration of the measurement of a_0 and a_f on the fracture surface.

Table 3
A summary of initial fracture toughness determined by the unloading compliance method.

Steel grade	Specimen No.	$\frac{a_0}{W}$	K_1	K_2	R^2	$\delta_{Ic-ASTM}$ (mm)	Mean of $\delta_{Ic-ASTM}$ (mm)	SD of $\delta_{Ic-ASTM}$ (mm)
G250	01	0.522	509.9435	0.2516	0.9962	0.6036	0.5816	0.0195
	02	0.542	501.5483	0.2888	0.9993	0.5849		
	03	0.573	486.3848	0.3218	0.9987	0.5563		
G350	01	0.544	450.3070	0.3723	0.9985	0.5052	0.5192	0.0133
	02	0.530	478.6645	0.3520	0.9956	0.5370		
	03	0.560	452.7771	0.3078	0.9972	0.5153		
PT460NR	01	0.493	600.7026	0.4609	0.9991	0.5731	0.5592	0.0104
	02	0.511	592.8254	0.5028	0.9994	0.5518		
	03	0.507	582.0754	0.4325	0.9979	0.5527		
A516-70	01	0.534	694.4360	0.3840	0.9927	0.6919	0.7182	0.0188
	02	0.523	720.6834	0.3821	0.9975	0.7278		
	03	0.510	725.0206	0.3105	0.9984	0.7349		

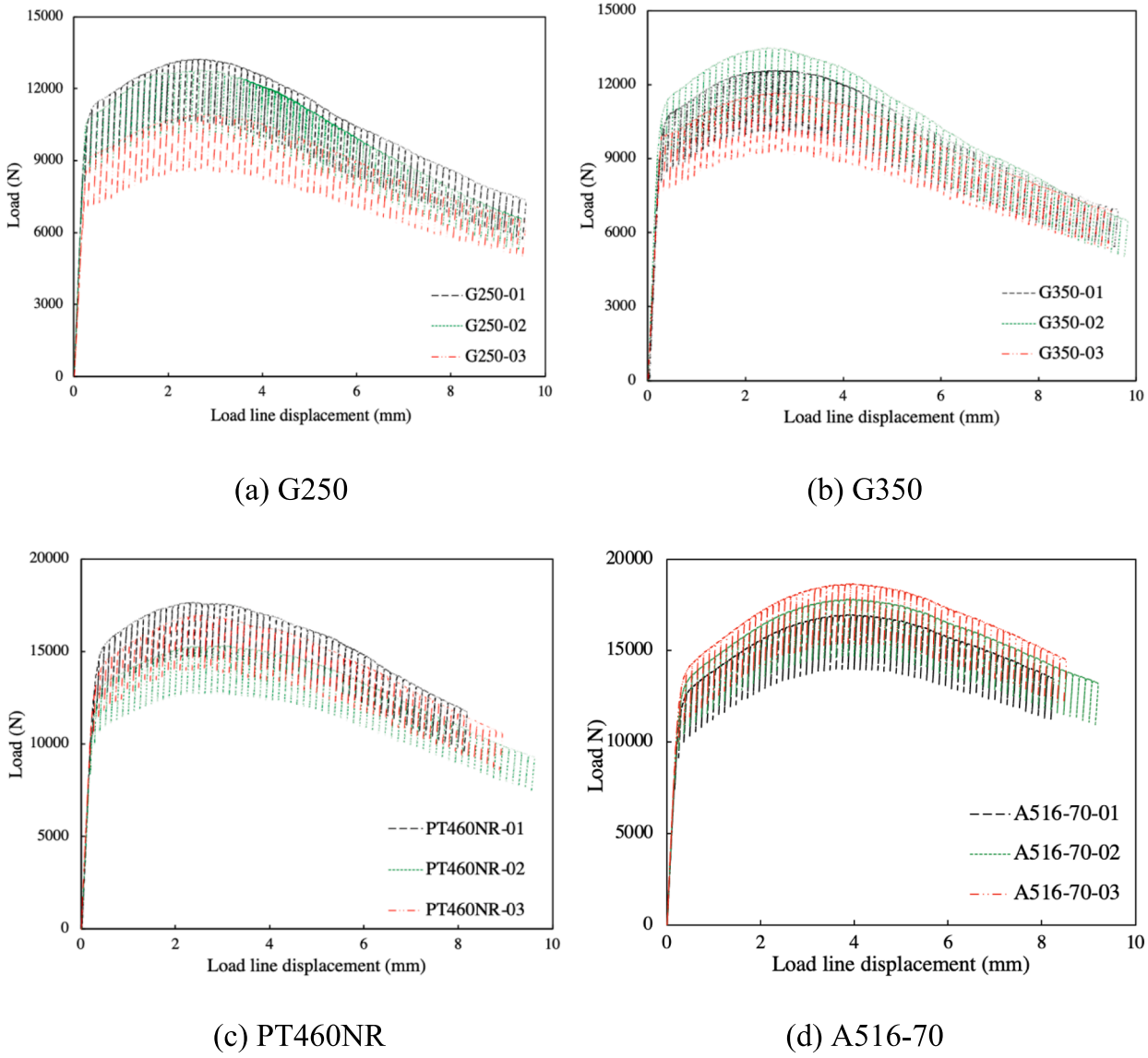

Fig. 7. Load-LLD curves obtained by the unloading compliance method for tested mild steel.

As per the preceding analysis, due to the consistency of initial fracture toughness values δ_{5c} with minimal dependency on the ratio of initial pre-crack lengths to width, and the proximity of $\delta_{Ic-\mathrm{ASTM}}$ values to those of δ_{5c}, the mean values of both δ_{5c} and $\delta_{Ic-\mathrm{ASTM}}$ are employed to investigate the influence of strain hardening on the assessment of initial fracture toughness in mild steel. This investigation studies the impacts of effective yield stress (σ_Y), strain hardening capacity ($1/n$) and yield offset ($\alpha\frac{\sigma_{ys}}{E}$) on the initial fracture toughness of mild steel.

3.3.1. *Effective yield stress*

The effective yield stress is one of the crucial factors in determining the initial fracture toughness of mild steel. As shown in Table 6, Despite having similar values of strain hardening exponent n (with a deviation value of 0.301 %) and dimensionless constant α (with a deviation value of 2.796 %), a comparison between G250 and PT460NR reveals differences in their respective values of initial fracture toughness. Specifically, as shown in Fig. 10, G250 exhibits a lower effective yield stress σ_Y and higher initial fracture toughness than PT460NR. The research conducted by Tvergaard and Hutchinson [36] indicates that this phenomenon can be attributed to the impact of effective yield stress. A higher effective yield stress imposes a limit on the extent of plastic deformation before the fracture initiation. Consequently, a lower amount of energy is required to be absorbed for the plastic deformation, resulting in a reduced material resistance to fracture and assisting the crack propagation. In addition, for ductile materials subjected to the mode-I loading conditions, fracture initiation and crack propagation are governed by the nucleation, growth, and coalescence of voids [42]. Specifically, voids form around inclusions or second-phase particles during the loading process. Then, plastic strain at the crack tip causes these voids to grow as the crack tip blunted, leading to voids linking and resulting in macroscopic crack propagation. According to the studies conducted by Rice and Rosengren [28], a larger stress around the crack tip can facilitate the nucleation of microcracks in materials, and also promote the growth and coalescence of voids.

Based on Table 4, for material G250 and PT46NR, the deviations in initial fracture toughness determined between the DIC technique-based method and the UC method are less than 3.0 %. Therefore, the initial fracture toughness determined by the DIC technique-based method has a good agreement with that of the UC method. Additionally, this value decreases as the effective yield stress increases. According to the ASTM E1820-21 standard [3], initial fracture toughness is determined as the intersection point of a 0.2 mm offset line and the *J-R* curve in the UC method. The slope of this offset line equals to $2\sigma_Y$. It can be concluded

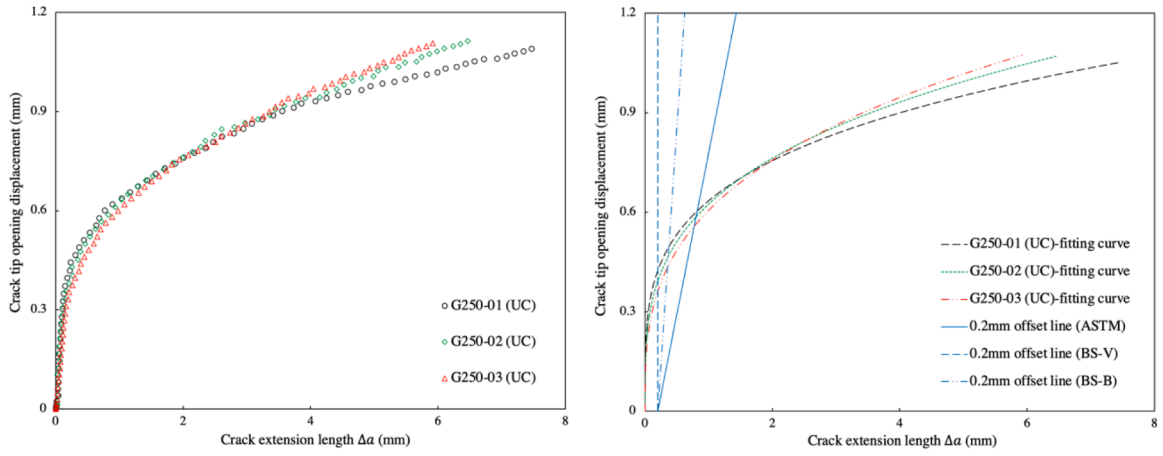

(a) G250

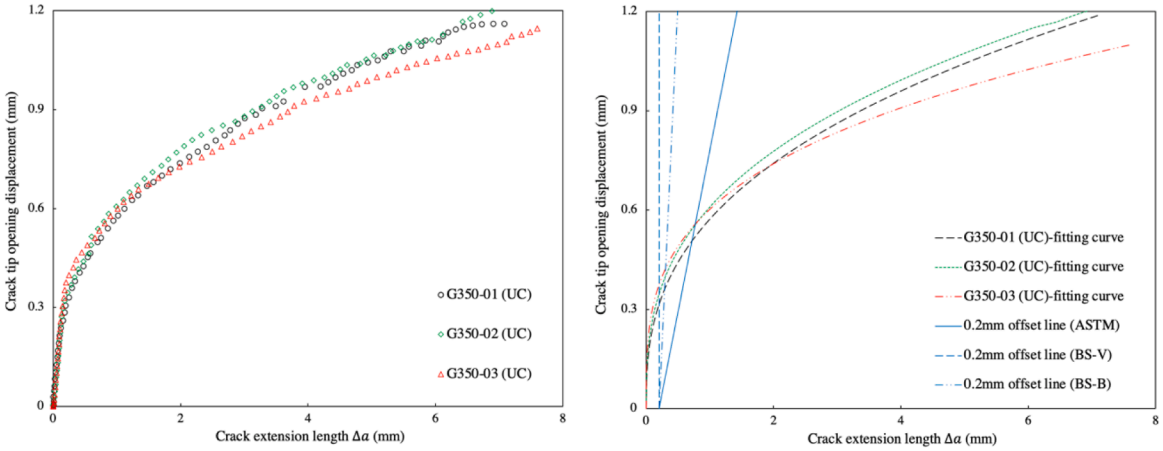

(b) G350

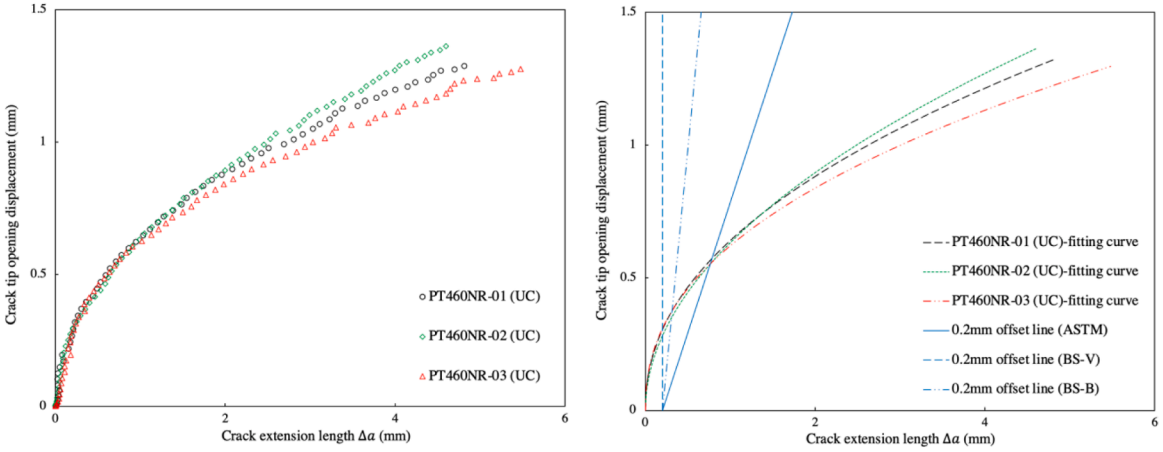

(c) PT460NR

Fig. 8. Construction of δ-R curves and determination of initial fracture toughness for tested mild steel.

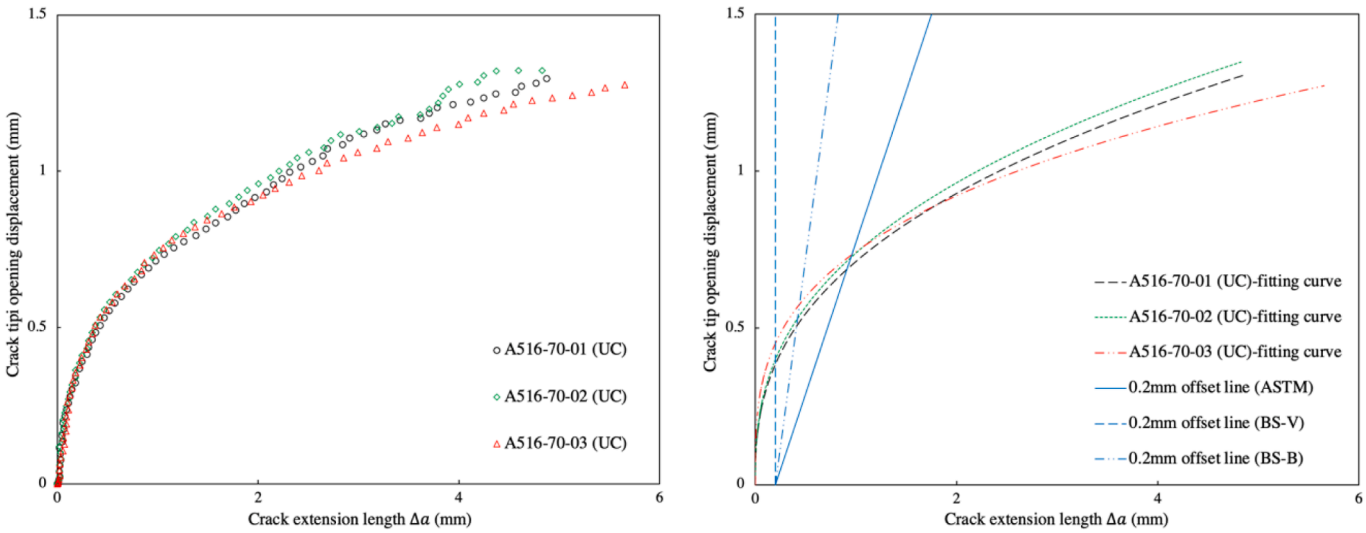

(d) A516-70

Fig. 8. (*continued*).

that the determination of initial fracture toughness in the UC method is influenced by effective yield stress, and the deviation between these two methods decreases with an increase in effective yield stress.

3.3.2. Strain hardening capacity

Strain hardening capacity is another crucial factor affecting the initial fracture toughness of mild steel. As shown in Table 5, while materials G250 and G350 have similar effective yield stress σ_Y (with a deviation value of 1.660 %) and yield offset $\alpha\sigma_{ys}/E$ (with a deviation value of 3.369 %), their initial fracture toughness values are significantly different. Specifically, compared to G250, G350 exhibits a higher strain hardening exponent (with a deviation value of 9.774 %) but lower initial fracture toughness (with a deviation value of about 11 %). As presented in Table 5 and Fig. 11, this phenomenon is also observed in the case of materials PT460NR and A156-70. These phenomena can be attributed to the influence of strain hardening capacity, as described by the parameter $1/n$. For the material with a higher strain hardening capacity (e.g., G250 and A516-70), a larger area of plastic deformation is formed around the crack tip because of harder strain localization [4]. Thus, a larger amount of energy needs to be dissipated before fracture initiation, leading to a higher material resistance to fracture initiation. Additionally, strain hardening capacity can reflect the level of crack tip blunting, i.e., a higher strain hardening capacity has a higher level of crack tip blunting. Since crack tip blunting can relieve the stress concentration around the crack tip, it will assist the material resistance to fracture initiation and crack extension, resulting in a higher initial fracture toughness.

Furthermore, based on Table 5, for all tested material, i.e., G250, G350, PT460NR and A516-70, the deviations in initial fracture toughness determined between the DIC technique-based method and the UC method are also less than 3.0 %. It further indicates that the initial fracture toughness determined by the DIC technique-based method has a good agreement with that of the UC method. Moreover, this value decreases with the increasing of strain hardening exponent n (i.e., decreasing of strain hardening capacity $1/n$). Consequently, the determination of initial fracture toughness in the UC method is also influenced by strain hardening capacity, and the deviation between these two methods decreases with a decrease in strain hardening capacity.

3.3.3. Yield offset

According to the data presented in Tables 4 and 5, the effective yield stress of PT460NR differs from that of G250 by approximately 18 %, while the mean initial fracture toughness of these two materials deviates by about 4 %. Comparing G250 and G350, the deviation in strain hardening exponent is approximately 10 %, while the deviation in mean initial fracture toughness between these two materials is about 11 %. Similarly, the strain hardening exponent deviation between PT460NR and A516-70 is about 18 %, and the mean initial fracture toughness deviation between these two materials is about 29 %. These findings suggest that the impact of strain hardening capacity ($1/n$), effective yield stress (σ_Y), and yield offset ($\alpha\sigma_{ys}/E$) on the initial fracture toughness of mild steel follows the order of $1/n > \sigma_Y > \alpha\sigma_{ys}/E$.

4. Further discussion

In this section, the discussions primarily focus on the factors that influence the accuracy of fracture toughness measurement in mild steel. Subsequently, potential areas for further research are proposed.

4.1. Crack path

In Table 3, the results reveal that the initial fracture toughness ($\delta_{Ic-ASTM}$) determined by intersecting δ-R curves with a 0.2 mm offset line, exhibits variability among duplicate specimens. This inconsistency may be attributed to the deviation in crack propagation paths. The crack propagation directions display an inclination with respect to the pre-crack direction, owing to the influence of the material's microstructure, e.g., crystal orientation, grain size and boundaries, second-phase particles, and inclusions [21,32]. A same value of crack extension length can be obtained from different crack paths. Consequently, it will incur different plastic deformation and necessitates the dissipation of different plastic energy for crack propagation. While the initial fracture toughness (δ_{5c}) determined by detecting the first occurrence of a sharp drop in strain near the crack tip, demonstrates consistency among duplicate specimens. This implies that with adequate quality of DIC painting and appropriate placement of points for strain measurement, the influence of the crack propagation path on the determination of initial fracture toughness can be considerably mitigated.

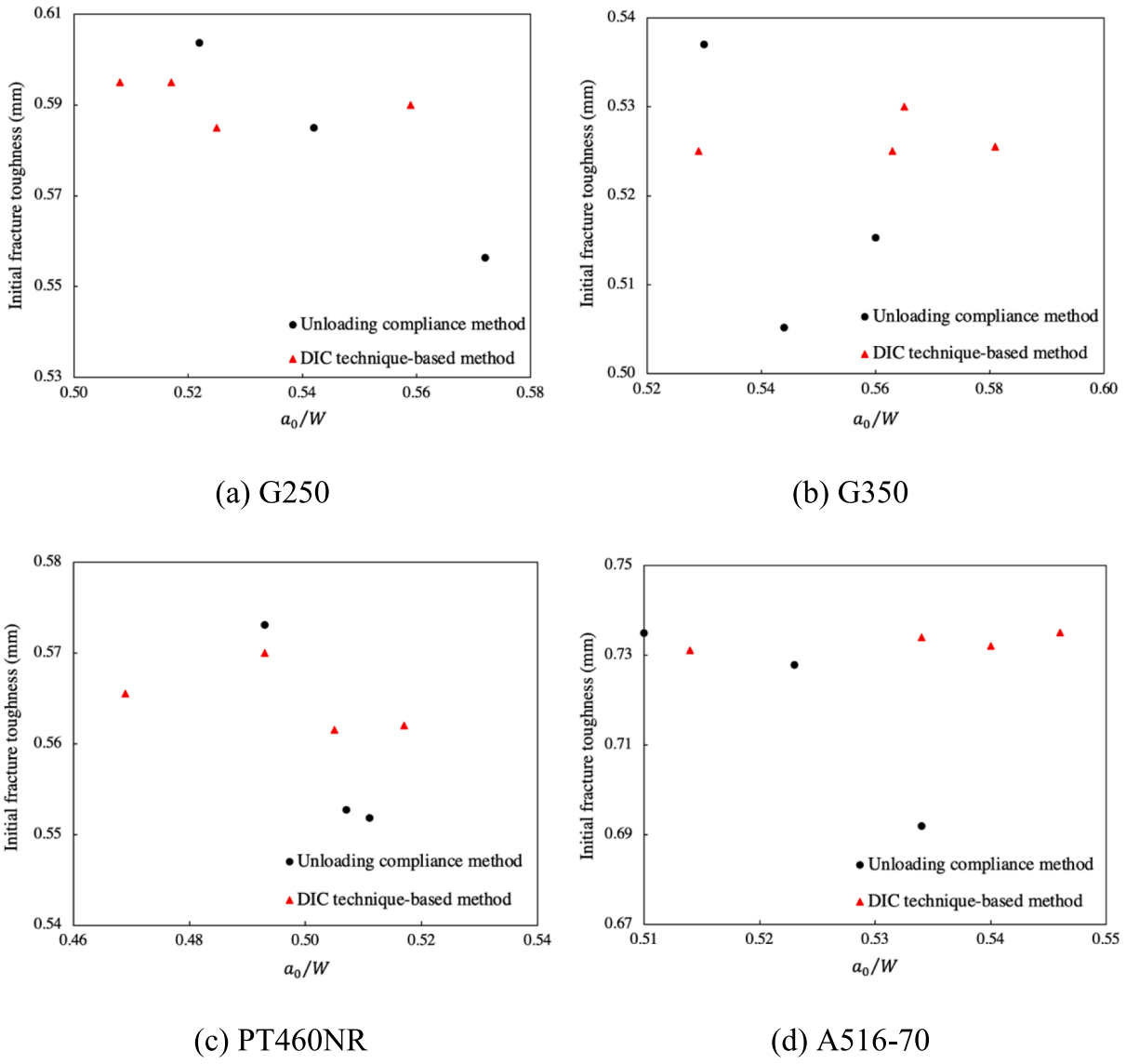

Fig. 9. A comparison of determined initial fracture toughness between DIC technique-based and UC methods.

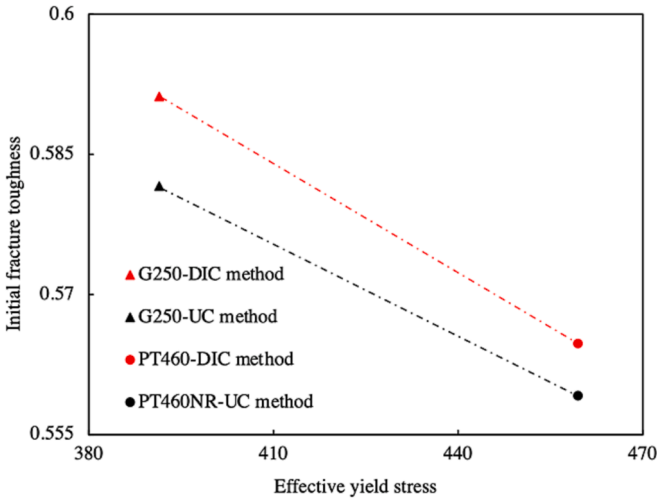

Fig. 10. Impact of effective yield stress on the initial fracture toughness.

Table 4
Impact of effective yield stress on the initial fracture toughness.

Material properties	σ_Y (MPa)	n	α	Mean of δ_{5c} (mm)	Mean of $\delta_{Ic-ASTM}$ (mm)	Deviation (%)
G250	391.5	6.65	6.08	0.5913	0.5816	1.668
PT460NR	459.5	6.67	5.91	0.5648	0.5592	1.001
Deviation (%)	17.369	0.301	2.796	4.482	3.851	–

4.2. Initial ratio of pre-crack length to width

As illustrated in Table 3, the values of initial fracture toughness ($\delta_{Ic-ASTM}$) determined by unloading compliance (UC) methods are different, likely due to differences in the initial pre-crack length (a_0) between duplicates. The pre-crack tip is commonly first generated in the mid-thickness of specimens. As the travelling microscope employed in this study can only monitor the pre-crack tip on the specimen surface, it is not possible to monitor the pre-crack tip in the mid-thickness of specimens. Consequently, it is not feasible to control the ratio of initial pre-crack length to width (a_0/W) to the same value. Furthermore, as

Table 5
Impact of strain hardening capacity on the initial fracture toughness.

Material properties	σ_{ys} (MPa)	σ_Y (MPa)	n	$\alpha\frac{\sigma_{ys}}{E}$ ($\times 10^{-3}$)	Mean of δ_{5c} (mm)	Mean of $\delta_{Ic-ASTM}$ (mm)	Deviation (%)
G250	336	391.5	6.65	9.822	0.5913	0.5816	1.668
G350	333	385.0	7.30	9.549	0.5264	0.5192	1.387
Deviation (%)	0.893	1.660	9.774	3.369	10.976	10.729	–
PT460NR	398	459.5	6.67	11.363	0.5648	0.5592	1.001
A516-70	401	472.0	5.45	11.608	0.7330	0.7182	2.061
Deviation (%)	0.754	2.720	18.291	2.156	29.834	28.433	–

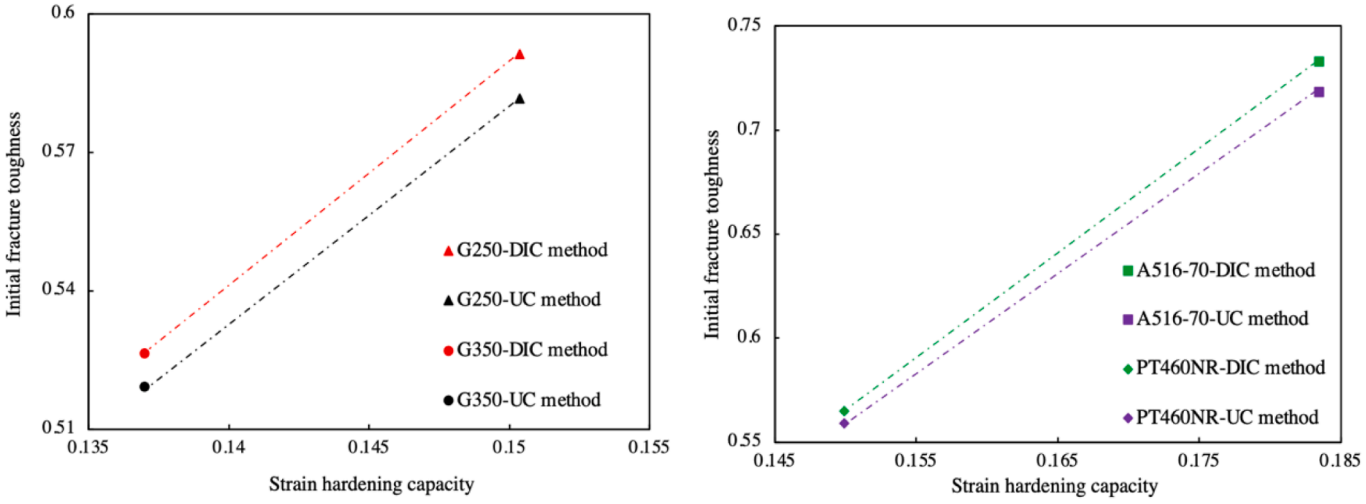

Fig. 11. Impact of strain hardening capacity on the initial fracture toughness.

shown in Fig. 10, the values of $\delta_{Ic-ASTM}$ are influenced by a_0/W. Specifically, with smaller a_0/W yielding larger $\delta_{Ic-ASTM}$. Shallow initial cracked specimens, with a higher a_0/W value, exhibit higher load-load line displacement curves (as shown in Fig. 7) and generate more plastic deformation around the crack tip [41], resulting in a greater amount of energy required to be absorbed before fracture initiation. In summary, since the determination of fracture toughness by the UC method relies on load-load line displacement curves that are affected by a_0/W, the values of initial fracture toughness obtained using this method will be dependent on a_0/W.

4.3. Standards

The approach for constructing the 0.2 mm offset line utilized in determining the initial fracture toughness varies across different standards. For clarity and distinction, the initial fracture toughness δ_{Ic} determined using the unloading compliance-based method is denoted as $\delta_{Ic-ASTM}$, $\delta_{Ic-BS(V)}$ and $\delta_{Ic-BS(B)}$, in accordance with the evaluation criteria of the ASTM E1820-21 standard [3] and [5] standard (British Standards Institution, 1997), respectively. A summary of δ_{Ic} determined by different standards in the UC method is presented in Table 6. It was found that the most conservative estimation is provided by $\delta_{Ic-BS(V)}$ in compliance with the [5] standard (British Standards Institution, 1997). Furthermore, combined with the data presented in Tables 4 and 5, it can be observed that the values of $\delta_{Ic-ASTM}$ are more closely aligned with those of δ_{5c}, owing to the fact that the influence of effective yield stress (σ_Y) is considered in the ASTM E1820-21 standard [3], as opposed to the [5] standard (British Standards Institution, 1997). Therefore, it can be

Table 6
A comparison of initial fracture toughness determined by different standards in the unloading compliance method.

Steel grade	Specimen No.	$\frac{a_0}{W}$	$\delta_{Ic-ASTM}$ (mm)	$\delta_{Ic-BS(V)}$ (mm)	Deviation (%)	Average (%)	$\delta_{Ic-BS(B)}$ (mm)	Deviation (%)	Average (%)
G250	01	0.522	0.6036	0.4240	29.755	32.467	0.4950	19.992	20.801
	02	0.542	0.5849	0.3930	32.809		0.4670	20.157	
	03	0.573	0.5563	0.3625	34.837		0.4325	22.254	
G350	01	0.544	0.5052	0.3150	37.648	33.513	0.3615	28.444	24.111
	02	0.530	0.5370	0.3460	35.568		0.3975	25.978	
	03	0.560	0.5153	0.3745	27.324		0.4230	17.912	
PT460NR	01	0.493	0.5731	0.3060	46.606	46.441	0.3765	34.305	34.342
	02	0.511	0.5518	0.2825	48.804		0.3490	36.752	
	03	0.507	0.5527	0.3100	43.912		0.3760	31.970	
A516-70	01	0.534	0.6919	0.3850	49.415	45.930	0.4325	38.792	35.757
	02	0.523	0.7278	0.3925	46.070		0.4670	35.834	
	03	0.510	0.7349	0.4240	42.305		0.4950	32.644	

inferred that the ASTM E1820-21 standard [3] is better suited for measuring the fracture toughness of mild steel.

4.4. Future studies

To ensure the safety of engineering structures, ASTM fracture test standards are designed to provide conservative and crack tip constraint-independent measurements of fracture toughness. These conservative values are obtained through stringent requirements on specimen preparation, such as using deeply pre-cracked specimens, imposing plane strain loading conditions, and specifying specific geometry and size criteria, among others. The degree of conservatism associated with these standards is however not quantified. In the real-world engineering applications, it is often not feasible to strictly adhere to these laboratory requirements. However, fracture toughness values obtained from laboratory tests are commonly utilized in practical applications, which will lead to a potential underestimation of structural integrity. Therefore, there is a need to develop effective methods that can accurately translate fracture toughness values measured from laboratory tests to practical engineering practices.

5. Conclusion

In this paper, the performance of the DIC technique-based fracture toughness method for determining the initial fracture toughness of mild steel has been studied. It has been achieved by comparing the results obtained from the DIC-technique based method with those of unloading compliance (UC) method. Furthermore, the effects of strain hardening on the fracture behaviour have been comprehensively investigated. The strain hardening effects are represented by strain hardening capacity ($1/n$), yield offset ($\alpha\sigma_{ys}/E$), and effect yield stress (σ_Y). The analysis of experimental results reveals that the DIC technique-based method exhibited good agreement with the UC method in determining the initial fracture toughness of mild steel. Notably, it demonstrated consistency without dependency on the ratio of initial pre-crack length to width (a_0/W). Additionally, the results indicated that the effects of strain hardening followed the order of strain hardening capacity ($1/n$) > effective yield stress (σ_Y) > yield offset ($\alpha\sigma_{ys}/E$). The ASTM E1820-21 standard is also found to be more suitable for evaluating the initial fracture toughness of mild steel than the [5] standard in the UC method. The findings presented in the paper provide a deep understanding of the performance of the DIC technique on the determination of initial fracture toughness of mild steel. They also point to a future research direction for improving the UC method without dependency on a_0/W. Furthermore, a comprehensive understanding of strain hardening effects on the fracture toughness of mild steel can help more accurate predictions of its fracture behaviour.

CRediT authorship contribution statement

Bohua Zhang: Conceptualization, Data curation, Formal analysis, Investigation, Methodology, Software, Validation, Visualization, Writing – original draft. **Weigang Wang:** Investigation, Methodology, Software, Writing – review & editing. **Haoran Lei:** Investigation, Software, Writing – review & editing. **Xiancun Hu:** Investigation, Methodology, Writing – review & editing. **Chun-Qing Li:** Writing – review & editing.

Declaration of Competing Interest

The authors declare that they have no known competing financial interests or personal relationships that could have appeared to influence the work reported in this paper.

Data availability

Data will be made available on request.

Acknowledgement

The authors gratefully acknowledge the financial support provided by the Australian Research Council through grants DP230100983 and IC230100015. The first author acknowledges the invaluable technical support provided by William Song from the material testing laboratory, Eric Gao from the heavy structure laboratory, and Paul Muscat from the manufacture & fabrication laboratory at RMIT. The first author also expresses gratitude to Belinda Domaille from the structural testing department at RMIT for her kind assistance with technical coordination.

Appendix A

The elastic $J_{el(i)}$ can be determined as follows:

$$J_{el(i)} = \frac{K_i^2(1-v^2)}{E} \tag{A 1.1}$$

with

$$K_i = \frac{P_i}{(BB_N W)^{1/2}} \frac{\left(2+\frac{\Delta a_{ci}}{W}\right)\left[0.886+4.64\left(\frac{\Delta a_i}{W}\right)-13.32\left(\frac{\Delta a_{ci}}{W}\right)^2+14.72\left(\frac{\Delta a_{ci}}{W}\right)^3-5.6\left(\frac{\Delta a_{ci}}{W}\right)^4\right]}{\left(1-\frac{\Delta a_{ci}}{W}\right)^{3/2}} \tag{A 1.2}$$

The plastic $J_{pl(i)}$ can be determined as follows [7]:

$$J_{pl(i)} = \left[J_{pl(i-1)} + \frac{\eta_{pl(i-1)}}{b_{i-1}} \frac{A_{pl(i)} - A_{pl(i-1)}}{B_N}\right]\left[1-\gamma_{i-1}\frac{\Delta a_{ci} - \Delta a_{c(i-1)}}{b_{i-1}}\right] \tag{A 1.3}$$

with

$$\eta_{pl(i-1)} = 2.0 + 0.522\left[W - \Delta a_{c(i-1)}\right]/W \tag{A 1.4a}$$

$$\gamma_{i-1} = 1.0 + 0.76\left[W - \Delta a_{c(i-1)}\right]/W \tag{A 1.4b}$$

$$A_{pl(i)} - A_{pl(i-1)} = \left[P_i - P_{i-1}\right]\left[V_{pl(i)} - V_{pl(i-1)}\right]/2 \tag{A 1.4c}$$

where $A_{pl(i)} - A_{pl(i-1)}$ represents the increment of plastic area that under the load-plastic LLD curve between the $(i-1)th$ and ith loading–unloading cycles, and $V_{pl(i)}$ denotes the plastic part of LLD at the beginning of ith loading–unloading cycle, i.e., $V_{pl(i)} = V_i - P_i C_{ci}$.

Appendix B

As per the ASTM E1820-21 standard [3], the crack extension length (Δa_i) at the beginning of the ith loading–unloading cycle can be estimated as follows:

$$\Delta a_i = \left(1.000196 - 4.06319u + 11.242u^2 - 106.043u^3 + 464.335u^4 - 650.677u^5\right)W \tag{A 2.1}$$

with

$$u = 1/\left[\left(B_e E C_i\right)^{0.5} + 1\right] \tag{A 2.2}$$

where the subscript (i) denotes the ith loading–unloading cycle, W is the width of the specimen, B_e is the effective specimen thickness which can be calculated as $B_e = B - (B - B_N)^2/B$ with B_N represented as the net thickness, and C_i represents the experimentally determined elastic compliance corresponding to ith loading–unloading cycle, i.e.,

$$C_i = \Delta V_i / \Delta P_i \tag{A 2.3a}$$

where V_i and P_i are the last data points of LLD and load, respectively, just before the initiation of the ith unloading process. When the effect of specimen rotation is considered, the corrected elastic compliance can be mathematically expressed as follows:

$$C_{ci} = \frac{C_i}{\left(\frac{H^*}{R_i}\sin\theta_i - \cos\theta_i\right)\left(\frac{D}{R_i}\sin\theta_i - \cos\theta_i\right)} \tag{A 2.3b}$$

where H^* represents the initial half-span of the loading points, i.e., the centre of pin holes. D represents one-half of the initial distance between the LLD measurement points. R_i represents the radius of rotation of the crack centreline, i.e., $R_i = (W + \Delta a_i)/2$, where Δa_i represents the uncorrected crack extension length determined from Equations (A1.1)–(1.3a) with $C_{ci} = C_i$. θ represents the angle of rotation of a rigid body element about the unbroken midsection line, i.e., $\theta = arcsin\left[\left(D + \frac{V_i}{2}\right)/\sqrt{D^2 + R_i^2}\right] - arctan(D/R_i)$, where V_i represents the measured LLD at the beginning of the ith loading–unloading cycle. Consequently, the rotation-corrected crack extension length (Δa_{ci}) can be calculated by substituting the elastic compliance C_i in Equation (A2.2) with the corrected elastic compliance C_{ci}.

References

[1] J. Abanto-Bueno, J. Lambros, Investigation of crack growth in functionally graded materials using digital image correlation, Eng. Fract. Mech. 69 (14–16) (2002) 1695–1711.
[2] T.L. Anderson, Fracture Mechanics: Fundamentals and Applications, CRC Press, 2017.
[3] ASTM E1820-21, 2021. Standard Test Method for Measurement of Fracture Toughness. ASTM International, West Conshohocken, PA.
[4] D. Bhattacharjee, J.F. Knott, Ductile fracture in HY100 steel under mixed mode I/mode II loading, Acta Metall. Mater. 42 (5) (1994) 1747–1754.
[5] BS 7448-4, 1997. Fracture Mechanics Toughness Tests: Part 4 Method for Determination of Fracture Resistance Curves and Initiation Values for Stable Crack Extension in Metallic Materials. British Standards Institution, p. t5.
[6] J. Chattopadhyay, Improved J and COD estimation by GE/EPRI method in elastic to fully plastic transition zone, Eng. Fract. Mech. 73 (14) (2006) 1959–1979.
[7] Clarke, G.A., JD, L., 1979. Evaluation of the J Integral for the Compact Specimen.
[8] Clarke, G.A., Andrews, W.R., Paris, P.C., Schmidt, D.W., 1976. Single specimen tests for J Ic determination. In: Mechanics of Crack Growth. ASTM International.
[9] Davis, J.R. (Ed.), 2004. Tensile Testing. ASM International.
[10] M.G. Dawes, Elastic-Plastic Fracture Toughness Based on the COD and J-Contour Integral Concepts, ASTM International, 1979, pp. 307–333.
[11] S.A. English, N.K. Arakere, Effects of the strain-hardening exponent on two-parameter characterizations of surface-cracks under large-scale yielding, Int. J. Plast. 27 (6) (2011) 920–939.
[12] H. Gao, C.Q. Li, W. Wang, Y. Wang, B. Zhang, Factors affecting the agreement between unloading compliance method and normalization method, Eng. Fract. Mech. 235 (2020) 107146.
[13] H. Gao, W. Wang, Y. Wang, B. Zhang, C.Q. Li, A modified normalization method for determining fracture toughness of steel, Fatigue Fract. Eng. Mater. Struct. 44 (2) (2021) 568–583.
[14] H. Gao, Y.F. Wu, C.Q. Li, Performance of normalization method for steel with different strain hardening levels and effective yield strengths, Eng. Fract. Mech. 218 (2019) 106594.
[15] E.E. Gdoutos, Fracture Mechanics: an Introduction, Vol. 263, Springer Nature, 2020.
[16] D. Hellmann, K.H. Schwalbe, Geometry and size effects on JR and δ-R curves under plane stress conditions, in: Fracture Mechanics: Fifteenth Symposium, ASTM International, 1984, January.
[17] R. Herrera, J.D. Landes, A direct JR curve analysis of fracture toughness tests, J. Test. Eval. 16 (5) (1988) 427–449.
[18] T. Hollstein, J.G. Blauel, On the relation of the crack opening displacement to the J-integral, Int. J. Fract. 13 (1977) 385–390.
[19] Irwin, G.R., 1997. Plastic zone near a crack and fracture toughness.
[20] Knott, J.F., 1973. Fundamentals of Fracture Mechanics. Gruppo Italiano Frattura.
[21] S. Kumar, W.A. Curtin, Crack interaction with microstructure, Mater. Today 10 (9) (2007) 34–44.
[22] J.D. Landes, J.A. Begley, ASTM STP 560, American Society for Testing and Materials, Philadelphia, PA, 1974, p. 170.
[23] C.Q. Li, Life cycle modelling of corrosion affected concrete structures – initiation, ASCE J. Mater. Civ. Eng. 15 (6) (2003) 594–601.
[24] Y. Liu, X. Zheng, S. Osovski, A. Srivastava, On the micromechanism of inclusion driven ductile fracture and its implications on fracture toughness, J. Mech. Phys. Solids 130 (2019) 21–34.
[25] R. McMeeking, D.M. Parks, On Criteria for J-dominance of Crack-tip Fields in Large-scale Yielding, ASTM International, 1979, pp. 175–194.
[26] P. Moore, A. Pargeter, Comparison of using the crack mouth displacement (CMOD) and load line displacement (LLD) methods in the determination of critical J integral in SENB specimens, Fatigue Fract. Eng. Mater. Struct. 41 (9) (2018) 1997–2009.
[27] X. Qian, W. Yang, Initiation of ductile fracture in mixed-mode I and II aluminum alloy specimens, Eng. Fract. Mech. 93 (2012) 189–203.
[28] J.R. Rice, G. Rosengren, Plane strain deformation near a crack tip in a power-law hardening material, J. Mech. Phys. Solids 16 (1) (1968) 1–12.
[29] R.O. Ritchie, Mechanisms of fatigue-crack propagation in ductile and brittle solids, Int. J. Fract. 100 (1999) 55–83.
[30] S.T. Rolfe, J.M. Barsom, Fracture and Fatigue Control in Structures: Applications of Fracture Mechanics, ASTM International, 1977.
[31] S. Roux, J. Réthoré, F. Hild, Digital image correlation and fracture: an advanced technique for estimating stress intensity factors of 2D and 3D cracks, J. Phys. D: Appl. Phys. 42 (21) (2009) 214004.

[32] K.H. Schwalbe, On the influence of microstructure on crack propagation mechanisms and fracture toughness of metallic materials, Eng. Fract. Mech. 9 (4) (1977) 795–832.
[33] K.H. Schwalbe, B.K. Neale, J. Heerens, The GKSS test procedure for determining the fracture behaviour of materials, EFAM GTP 94 (1994) GKSS.
[34] C.F. Shih, M.D. German, Requirements for a one parameter characterization of crack tip fields by the HRR singularity, Int. J. Fract. 17 (1981) 27–43.
[35] M.A. Sutton, J.J. Orteu, H. Schreier, Image Correlation for Shape, Motion and Deformation Measurements: Basic Concepts, Theory and Applications, Springer Science & Business Media, 2009.
[36] V. Tvergaard, J.W. Hutchinson, The relation between crack growth resistance and fracture process parameters in elastic-plastic solids, J. Mech. Phys. Solids 40 (6) (1992) 1377–1397.
[37] K. Van Minnebruggen, M. Verstraete, S. Hertelé, W. De Waele, Evaluation and comparison of double clip gauge method and delta 5 method for CTOD measurements in SE (T) specimens, J. Test. Eval. 44 (6) (2016) 2414–2423.
[38] W.G. Wang, A. Zhou, G.Y. Fu, C.Q. Li, D. Robert, M. Mahmoodian, Evaluation of stress intensity factor for cast iron pipes with sharp corrosion pits, Eng. Fail. Anal. 81 (2017) 254–269.
[39] B. Zhang, W. Wang, Y. Li, H. Lei, C.Q. Li, A primary relationship between critical strain energy density and fracture toughness of mild steel, Theor. Appl. Fract. Mech. (2023) 104048.
[40] H. Zhang, G. Huang, H. Song, Y. Kang, Experimental investigation of deformation and failure mechanisms in rock under indentation by digital image correlation, Eng. Fract. Mech. 96 (2012) 667–675.
[41] X.K. Zhu, J.A. Joyce, J-Resistance curve testing of HY80 steel using SE (B) specimens and normalization method, Eng. Fract. Mech. 74 (14) (2007) 2263–2281.
[42] X.K. Zhu, J.A. Joyce, Review of fracture toughness (G, K, J, CTOD, CTOA) testing and standardization, Eng. Fract. Mech. 85 (2012) 1–46.
[43] ASTM E8, E8M-16a, Standard test methods for tension testing of metallic materials, ASTM International, West Conshohocken, 2016.
[44] J. Ast, M. Ghidelli, K. Durst, M. Göken, M. Sebastiani, A.M. Korsunsky, A review of experimental approaches to fracture toughness evaluation at the micro-scale, Materials Design 173 (2019) 107762.
[45] D. Frómeta, S. Parareda, A. Lara, S. Molas, D. Casellas, P. Jonsén, J. Calvo, Identification of fracture toughness parameters to understand the fracture resistance of advanced high strength sheet steels, Engineering fracture mechanics 229 (2020) 106949.
[46] J.A. Joyce, R.E. Link, Application of two parameter elastic-plastic fracture mechanics to analysis of structures, Engineering fracture mechanics 57 (4) (1997) 431–446.
[47] A.A. Wells, Application of fracture mechanics at and beyond general yielding, British Welding Journal 10 (1963).